

Role of electron tunneling in the nonlinear response of plasmonic nanogapsGarikoitz Aguirregabiria,¹ Dana Codruta Marinica,² Ruben Esteban,^{3,4} Andrey K. Kazansky,^{3,4} Javier Aizpurua,^{1,4} and Andrei G. Borisov^{2,4}¹*Material Physics Center CSIC-UPV/EHU, Paseo Manuel de Lardizabal 5, 20018 Donostia-San Sebastián, Spain*²*Institut des Sciences Moléculaires d'Orsay, UMR 8214 CNRS-Université Paris-Sud, Bât. 520, 91405 Orsay Cedex, France*³*IKERBASQUE, Basque Foundation for Science, Maria Diaz de Haro 3, 48013 Bilbao, Spain*⁴*Donostia International Physics Center DIPC, Paseo Manuel de Lardizabal 4, 20018 Donostia-San Sebastián, Spain*

(Received 14 December 2017; revised manuscript received 14 February 2018; published 19 March 2018)

We report on the theoretical study of the second and third harmonic generation in plasmonic dimer nanoantennas with narrow gaps. Our study is based on the time dependent density functional theory. This allows us to address the nonlinear response of a tunneling junction in a subnanometric plasmonic gaps with a quantum calculation, which goes beyond conventional classical local and nonlocal treatments. We demonstrate that the nonlinear electron transport in a plasmonic junction, associated to the corresponding strong field enhancement in the narrow gap, allows to reach orders of magnitude enhancement in the efficiency of the second and third harmonic generation. Depending on the size of the junction and the frequency of the fundamental incident wave, we show that the frequency conversion in plasmonic dimer gaps can be determined by (i) the intrinsic nonlinearity of each individual nanoparticle, (ii) the nonlinear ac tunneling current across the gap, and (iii) the resonant excitations of the plasmon modes of the dimer. The study of the nonlinear response of plasmonic gaps within a full quantum treatment allows us to understand the fundamental mechanisms of nonlinearity in nanoplasmonics.

DOI: [10.1103/PhysRevB.97.115430](https://doi.org/10.1103/PhysRevB.97.115430)**I. INTRODUCTION**

Nonlinear optical effects in nanoscale devices allow to control the electromagnetic fields of light at dimensions well below the wavelength, making them the focus of an intense research effort [1–5]. Indeed, the nonlinear response plays an important role in numerous applications of nanophotonics devoted to information transfer [5–10]. Moreover, frequency conversion and generation of high harmonics can be used for (bio-)imaging [11–14], metrology and sensing [15–18], and generation of the attosecond XUV laser pulses [19,20]. The latter allowed spectacular progress in direct time-domain access to electronic processes in atoms, molecules, and solids [20,21]. However, optical nonlinearities are usually weak, and therefore the nonlinear responses associated to them are orders of magnitude smaller than the linear ones.

Plasmonics offers a way to overcome this difficulty since many experimental and theoretical works addressed plasmon-enhanced nonlinear effects at metallic surfaces, nanoparticles, and in artificially created nanomaterials [5,10,22–34]. The common understanding provided by these approaches is that the coupling of light with collective electron oscillations in the metal (plasmons) results in the enhancement of the near fields in the proximity of metallic surfaces, which can be utilized to boost nonlinear effects. Recent developments also demonstrate the role of plasmon excitations in the nonlinear response of graphene nanostructures [35–37]. Among others, plasmonic systems with narrow gaps have received a lot of attention as platforms to effectively support nonlinear optical processes because of their ability to strongly enhance electromagnetic field in the gap region [5,27–30,38–51]. The classical electromagnetic theory is routinely applied to explain many of the

experimental data and to predict the nonlinear properties of nanostructures using perturbative and model approaches. Thus it has been shown that an efficient frequency conversion can be obtained by fulfilling appropriate symmetry constraints, and choosing the frequency of the fundamental incident wave or its corresponding high harmonic in resonance with a suitable plasmonic mode of the system [29–34,48–61].

In this context, the quantum regime of plasmonics where the atomic scale becomes relevant is an interesting platform to explore nonlinear responses. Indeed, advances in fabrication techniques have allowed to engineer plasmonic structures with nanometer control of their geometry. Dimer plasmonic antennas with nanometer and subnanometer gaps, for instance, have reached the regime where the *linear optical response* is sensitive to quantum effects such as nonlocal screening and electron tunneling between the constituting nanoparticles [62–77]. This brings the question about the impact of quantum effects on nonlinear processes in plasmonic structures with (sub-)nanometer gaps, and their ability to strengthen the associated *nonlinear optical response*. Thus the coupling of photons with tunneling electrons is shown to provide ultracompact sources for light and plasmon generation in tunneling configurations [78–81]. This effect can become a source of frequency conversion due to the strong sensitivity of the tunneling process to the potential barrier across the junction and to the variation of the tunneling barrier with the optical bias. Optical rectification, as studied in narrow plasmonic gaps formed by the STM, molecule functionalized, or break junctions [41,82–84], is one of the examples of nonlinearity associated to the tunneling current and, *a priori*, it is accompanied by second-harmonic generation.

The presence of the high harmonics in the tunneling current has been studied in the context of the theory of photoassisted electron transport (PAT) [85–89], particularly well developed in the THz frequency range for the semiconductor structures. At optical frequencies, the nonlinearity of the tunneling current was demonstrated using time-dependent density functional theory (TDDFT) calculations for the case of a plasmonic dimer formed by spherical nanoparticles [67,69]. Recently reported hydrodynamic methods demonstrate the impact of the nonlocal screening on the nonlinear response of individual nanoparticles [60,90–92], and a model study based on the theory of PAT addressed the effect of tunneling in the nonlinear response of the gap nanoantenna [93–96]. However, a parameter-free quantum approach that allows to elucidate the rich variety of effects in the nanogap plasmonic system and the contribution of the different mechanisms driving the optical frequency conversion has not been attempted so far. At the same time, the design of the efficient nonlinear devices requires understanding of the respective role of the field enhancement, plasmon resonances, intrinsic nonlinearity of metal nanoparticles, and the nonlinear electron transport through narrow gaps.

The present work aims at answering the above question by using TDDFT [97,98] calculations of the second and third harmonic generation from plasmonic dimer nanoantennas with narrow gaps. TDDFT provides a time-domain access to the quantum dynamics of the electron density of the system and thus allows for a nonperturbative treatment of nonlinear effects [99]. At variance with the model-Hamiltonian approaches within PAT, the TDDFT is a parameter-free treatment (as far as the potential acting on the valence electrons is set) that naturally includes the nonlocal screening and tunneling effects, essential in the case of metal nanoparticles. By considering a variety of geometries, different materials, and a wide range of junction sizes, we isolate different regimes of frequency conversion in structures with narrow plasmonic gaps. We analyze in detail the second and third harmonic generation in such situation, and show that under certain conditions the nonlinear tunneling current through the potential barrier between nanoparticles can provide a dominant contribution to the nonlinear response with up to two orders of magnitude increase of the frequency conversion efficiency. We also demonstrate that because of the role of the plasmon resonances the dimer configuration does not necessarily provides a gain in efficiency of the nonlinear process as compared to the pair of noninteracting nanoparticles.

The paper is organized as follows. The systems under study and the TDDFT approach are introduced in Sec. II. Sections III and IV are devoted to the results and their discussion. In particular, the role of quantum tunneling in the nonlinear response of the system is detailed in Sec. IV. The summary and conclusions of this work are given in Sec. V. Atomic units are used throughout the paper unless otherwise stated.

II. METHODS

To reveal the role of tunneling effects, field enhancement, and plasmon modes in the generation of frequency conversion, we perform TDDFT calculations of the nonlinear optical response in metal dimer structures with vacuum gap and with different geometries, as sketched in Fig. 1. The width of the

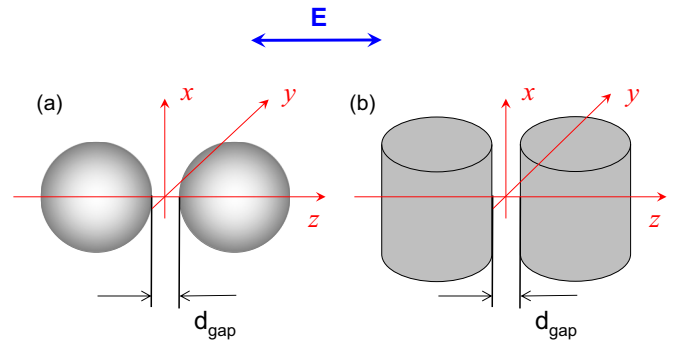


FIG. 1. Sketch of the studied systems. (a) Spherical Al nanoparticle dimer. An individual nanosphere has a radius of $R_{\text{sph}} = 11 \text{ \AA}$ and comprises 1012 electrons. (b) Dimer of Na cylinders, infinite along x axis. An individual cylinder has a radius $R_{\text{cyl}} = 30.7 \text{ \AA}$ and comprises 800 electrons per 1 nm length. The origin of coordinates is at the middle of the junction and the dimer z axis is such that the $(x, y, z = 0)$ plane is the symmetry plane of the system. The incident electromagnetic field is a plane wave polarized along the z axis and propagating along the y axis.

gap, d_{gap} , has been varied to cover all the interaction regimes, from a touching geometry to well-separated, weakly coupled nanoparticles. We consider a spherical nanoparticle dimer and a dimer formed by infinitely long cylindrical nanowires. The field of the fundamental incident wave is polarized along the dimer z axis, as sketched in the figure. The spherical nanoparticle and the cylindrical nanowire dimer geometries allow for a strong field enhancement in the junction and feature multitude of bonding and charge-transfer plasmon modes [64–70,100,101]. We have also considered the case of the parallel infinite Na metal slabs separated by the narrow vacuum gap. Each slab has the width $\ell = 100 \text{ \AA}$ and comprises 300 electrons per nm^2 area. In this system, the field in the junction is not enhanced, and only one plasmon mode close to the bulk plasmon frequency can be excited [102]. Therefore auxiliary calculations with parallel metal slabs were performed to confirm the importance of the field enhancement for the strong contribution of the nonlinear electron tunneling to frequency conversion by the system.

Our choice of the description of the metal nanoparticles is determined by several considerations. First, the focus of the present contribution is on the nonlinear dynamics of the conduction electrons, and in particular on the role of the electron tunneling across the gap between the nanoparticles. Second, the description of the metal nanoparticles needs to allow an efficient implementation of the TDDFT approach so that the nonlinear response can be obtained for relatively large nanoparticles with well established plasmon modes. We thus adopt the free-electron jellium model [103] (JM) of metal. Similar to the hydrodynamic treatments [60,90–92], this approach does not capture excitations involving electrons from the localized bands, as, e.g., a d band in case of noble metals. At the same time, the JM is well suited to describe the dynamics of valence electrons. In particular, the JM along with the TDDFT approach allow to account for the electron spill-out, tunneling, nonlocal response, and photon assisted transport, effects of paramount importance for electron-photon coupling in narrow

gaps. The JM has been often considered to elucidate robust quantum effects in the linear and nonlinear plasmon response as confirmed by *ab initio* and experimental results [66–77].

Within the JM the lattice ions are represented by a uniform positive background charge of density $n_+ = (\frac{4\pi}{3}r_s^3)^{-1}$, with r_s being the Wigner-Seitz radius. We use the value $r_s = 2.07 a_0$ which corresponds to the Al metal (spherical dimer), and $r_s = 4 a_0$ for the Na metal (cylindrical dimer, parallel slabs). Here, $a_0 = 0.053$ nm is the Bohr radius. While being the prototype of free-electron metals with valence electrons well described within the JM [103–107], Na and Al are characterized by very different electron densities. As a consequence, the bulk plasmon frequencies differ by nearly a factor of three which allows us to check the robustness of the observed effects. The Na metal nanoparticles feature plasmon modes in a frequency range similar to that of gold and silver nanoparticles and have been often used as a prototype to study quantum effects [67–70]. Al, on the other hand, attracts a growing attention in the plasmonics community owing to the presence of its plasmon resonances in the UV frequency range [26,33,108,109].

The real-time calculations of the electron density dynamics triggered by an external incident electromagnetic pulse are performed within the Kohn-Sham (KS) scheme [110] of TDDFT using the adiabatic local density approximation (ALDA) [97] for the exchange-correlation potential. The details of the numerical implementation of the method are given in Refs. [67,68,111] so that only a brief discussion will be presented here. The time-dependent electron density $n(\mathbf{r}, t) = \sum_{j \in \text{occ}} \chi_j |\psi_j(\mathbf{r}, t)|^2$ is given by the sum over all initially occupied KS orbitals $\psi_j(\mathbf{r}, t)$, where the χ_j multiplier accounts for the spin and symmetry degeneracy. The KS orbitals evolve in time according to the Schrödinger-type equations

$$i \partial_t \psi_j(\mathbf{r}, t) = [\hat{T} + V_H(\mathbf{r}, t) + V_{XC}(\mathbf{r}, t) + V_{\text{ext}}(\mathbf{r})] \psi_j(\mathbf{r}, t), \quad (1)$$

where \hat{T} is the kinetic energy operator, V_H the Hartree potential, V_{XC} is the exchange-correlation potential, and V_{ext} is the external potential. Equations (1) are solved on a mesh of spatial points using split-operator time propagation and pseudospectral techniques [112,113].

We use the velocity gauge with $\hat{T} = \frac{1}{2}[-i\nabla + \mathbf{A}(t)]^2$. The vector potential $\mathbf{A}(t)$ is defined through $\mathbf{E}(t) = -\partial_t \mathbf{A}(t)$, and the field $\mathbf{E}(t)$ of the incident Gaussian electromagnetic pulse is given by

$$\mathbf{E}(t) = \hat{e}_z E_0 \cos(\omega t) e^{-\frac{(t-t_0)^2}{\tau}}. \quad (2)$$

Here, \hat{e}_z is the unit length vector along the z axis. The pulse duration 2τ is set large enough (typically six laser periods) so that well-resolved harmonics can be observed in the spectrum of the induced dipole. Results presented below are obtained with a field amplitude $E_0 = 1.5 \times 10^{-3}$ a.u., which corresponds to an average power density of the incident pulse of 10^{11} W/cm². Different values of E_0 were also used to confirm the $\mathcal{I}_{n\omega} \propto E_0^{2n}$ scaling of the intensity $\mathcal{I}_{n\omega}$ of the n th harmonic.

The Hartree potential is obtained from the total charge density solving Poisson's equation $\Delta V_H = 4\pi[n_+(\mathbf{r}) - n(\mathbf{r}, t)]$. Retardation effects are neglected because of the small particle sizes considered here. The exchange-correlation potential of

Gunnarson and Lundqvist [114] is used in our study. Finally, the external potential, $V_{\text{ext}}(\mathbf{r}) = E_p z$, describes the electron interaction with a dc field applied along the z axis. For the dimer formed by identical free-electron metal nanoparticles the second harmonic generation is a symmetry forbidden process [30,45,46]. However, this process can be induced using a polarising field E_p [38,115–117] that allows to actively control the intensity of the second harmonic generation [117]. The results shown below are obtained for polarizing field $E_p = 1.05 \times 10^{-4}$ a.u. In the calculations of the third harmonic, no dc polarizing field is applied, $E_p = 0$.

The frequency-resolved quantities such as the induced dipole \mathbf{p}_Ω , the z -component of the induced field in the middle of the junction E_Ω^z , current through the middle of the junction I_Ω , current density $\mathbf{j}_\Omega(\mathbf{r})$, or induced charge densities $\Delta n_\Omega(\mathbf{r})$, are obtained from the corresponding time-dependent quantities using the time-to-frequency Fourier transform. Thus considering that the relevant sizes of the dimers under the study are much smaller than the optical wavelength, the nonlinear response of the nanostructure can be adequately described by the dipole induced at the corresponding frequency $p_{n\omega}$ (with $n = 2$ and 3), given by

$$p_{n\omega} = \int_0^T e^{i\Omega t} e^{-\frac{(t-t_0)^2}{\tau}} p(t) dt, \quad \Omega = n\omega \quad (3)$$

(in what follows we will not use the vector notations for the dipoles because for symmetry reasons only the dipole along the z axis can be induced in the systems considered here). In Eq. (3), T is a large enough (though finite) propagation time, and $p(t)$ is the time-dependent dipole of the nanostructure

$$p(t) = - \int z \Delta n(\mathbf{r}, t) d^3 \mathbf{r}. \quad (4)$$

It is obtained from the induced electron density $\Delta n(\mathbf{r}, t)$ calculated with TDDFT in response to the incident electromagnetic pulse. Alternatively, assuming the $\exp(-i\omega t)$ time dependence, the $p_{n\omega}$ can be obtained from the TDDFT result for the z component of the harmonic current density $j_{z,n\omega}(\mathbf{r})$ [118],

$$n\omega p_{n\omega} = i \int j_{z,n\omega}(\mathbf{r}) d^3 \mathbf{r}. \quad (5)$$

We have explicitly checked that Eqs. (3) and (5) yield the same result.

The nonlinear polarizations and currents $p_{2\omega}$, $p_{3\omega}$, $j_{z,2\omega}(\mathbf{r})$, and $j_{z,3\omega}(\mathbf{r})$ are orders of magnitude smaller than the induced dipole and current density at the fundamental frequency p_ω , $j_{z,\omega}(\mathbf{r})$. In performing the Fourier analysis of the time-dependent quantities, we then use a Gaussian filter of width $\Delta \geq \tau$ as in Eq. (3). This approach allows to improve the convergence of the spectral features at harmonic frequencies, and it is particularly appropriate for the excitation of the dimer nanoantenna far from the plasmon resonance where the dipolar polarization is only induced during the optical pulse (in practice we set $\Delta = \tau$ in this case). In the cases where the harmonic frequency matches some plasmon mode of the dimer, the nonlinear dipole is enhanced, and it can be reliably extracted without using the filter [Δ parameter is set to infinity in Eq. (3)].

In Fig. 2, we show an example of the spectral analysis of the dipolar polarization of a cylindrical nanoparticle dimer.

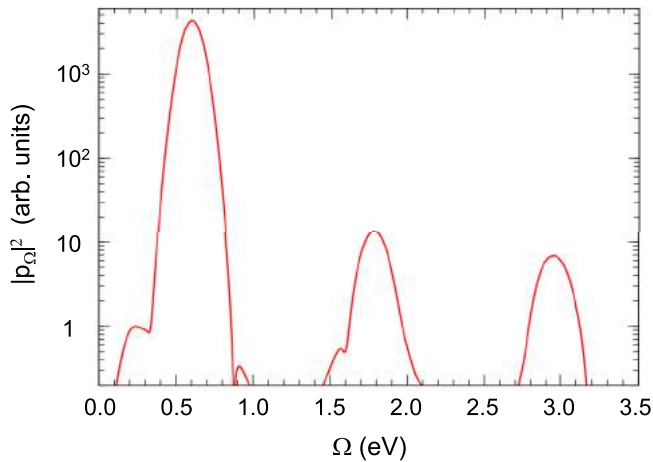


FIG. 2. Spectral analysis of the z component of the induced dipole for a dimer of cylindrical Na nanoparticles separated by the junction of the width $d_{\text{gap}} = 3.5 \text{ \AA}$. Results of the TDDFT calculations are shown as a function of the frequency Ω . The incident Gaussian electromagnetic pulse has carrier frequency $\omega = 0.6 \text{ eV}$ and duration $2\tau = 40 \text{ fs}$.

The main peak in Fig. 2 corresponds to the polarization at the fundamental frequency, and the third and fifth harmonics are clearly distinguishable (only odd harmonics can be obtained in this case as no polarizing field is applied).

From the nonlinear dipole $p_{n\omega}$, the power radiated by the nanostructure at harmonic frequency $\mathcal{I}_{n\omega}$ can be obtained as

$$\mathcal{I}_{n\omega} = \frac{(n\omega)^4}{3c^3} |p_{n\omega}|^2, \quad (6)$$

where c is the speed of light in vacuum. Within the perturbative regime the nonlinear dipolar polarization of the nanostructure can be characterized by the third-order hyperpolarizabilities: $\alpha^{(3)}(2\omega) \equiv \alpha^{(3)}(2\omega; \omega, \omega, 0)$ and $\alpha^{(3)}(3\omega) \equiv \alpha^{(3)}(3\omega; \omega, \omega, \omega)$,

defined with the following relations:

$$\begin{aligned} p_{2\omega} &= \alpha^{(3)}(2\omega) E_{\omega}^2 E_p, \\ p_{3\omega} &= \alpha^{(3)}(3\omega) E_{\omega}^3. \end{aligned} \quad (7)$$

By performing the TDDFT calculations for different power of the incident Gaussian pulse and strength of the polarizing field, we have explicitly checked that Eq. (7) holds. The hyperpolarizabilities can thus be obtained by inverting Eq. (7) with use of the values of $p_{n\omega}$ calculated within TDDFT.

III. LINEAR RESPONSE

Understanding of the main phenomena underlying the dependence of the nonlinear response on the frequency of the fundamental wave and on the size of the gap requires characterization of the linear optical properties of the system. For the dimer configuration, the linear optical response including the effects of quantum tunneling and nonlocality has been addressed in great detail in a number of studies [64–70, 100, 101]. Therefore only a brief discussion of the main features will be presented here.

The optical absorption cross section σ calculated with TDDFT for the Na nanowire dimer and Al nanosphere dimer in vacuum is shown in Figs. 3(a) and 3(b) as a function of the width of the gap d_{gap} and the frequency ω of the incident z -polarized plane wave (see Fig. 1). In Fig. 3(c), we show the d_{gap} dependence of the field enhancement, and of the ac electron current through the middle junction of the Na cylinder dimer. Results are presented for several selected frequencies relevant for the calculation of the frequency conversion below. The field enhancement is defined as $R_E = |E_{\omega}^g/E_{\omega}|$, where E_{ω} and E_{ω}^g are given by the Fourier transforms of the incident pulse, and of the field induced by the nanostructure in the middle of the junction, respectively. The ac electron current

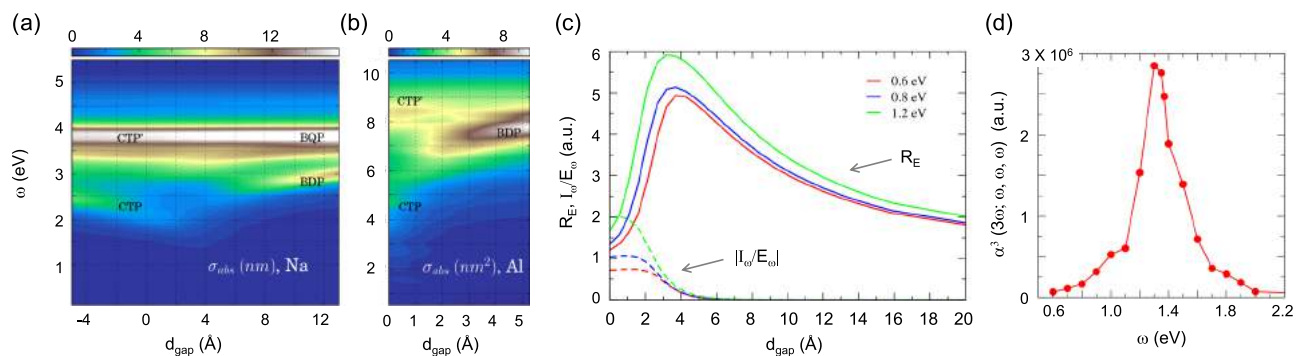


FIG. 3. [(a) and (b)] Color plots of the optical absorption cross section σ of a dimer of cylindrical Na (a) and spherical Al nanoparticles (b). TDDFT results are presented as a function of the size of the gap between nanoparticles d_{gap} and frequency of the incident plane wave ω . Labels indicate the plasmon modes responsible for the absorption resonances: bonding dipole plasmon (BDP), bonding quadrupole plasmon (BQP), the lowest (dipole) charge transfer plasmon (CTP), and the higher-energy charge transfer plasmon (CTP'). (c) Cylindrical Na dimer. The gap-size dependence of the enhancement of the incident field $R_E = |E_{\omega}^g/E_{\omega}|$ (solid lines) and of the amplitude of the normalized ac current $|I_{\omega}/E_{\omega}|$ between nanoparticles (dashed lines). The TDDFT results are obtained in the middle of the gap for different frequencies of the linearly polarized incident electromagnetic wave $\omega = 0.6 \text{ eV}$ ($\lambda = 2066 \text{ nm}$), $\omega = 0.8 \text{ eV}$ ($\lambda = 1550 \text{ nm}$), and $\omega = 1.2 \text{ eV}$ ($\lambda = 1033 \text{ nm}$) as explained in the insert. Here, E_{ω} is the incident field, E_{ω}^g is the induced ac field in the middle of the gap, and I_{ω} is the electron current through the gap at optical frequency. (d) Hyperpolarizability $\alpha^{(3)}(3\omega)$ of an individual Na nanowire. The values are given in atomic units (a.u.). The relation $1 \text{ esu} = 0.1985 \times 10^{40} \text{ a.u.}$ can be used for conversion of the third-order hyperpolarizability to electrostatic units (esu).

through the middle of the junction is given by

$$I_\omega = \hat{e}_z \int dx \int dy \mathbf{j}_\omega(x, y, z = 0), \quad (8)$$

and in Fig. 3(c) it is normalized to the field of the incident pulse (the $|I_\omega/E_\omega|$ quantity is shown).

For large gap widths (capacitive coupling between nanoparticles), the absorption resonances correspond to the excitation of the bonding plasmon modes [bonding dipole plasmon (BDP), bonding quadrupole plasmon (BQP), etc.]. These modes are formed by the hybridization between the dipolar and higher momentum plasmon modes of the individual nanoparticles [101]. As the width of the gap d_{gap} decreases, the bonding plasmon modes experience a red shift because of the attractive interaction between the charges of opposite sign induced at facing metal surfaces across the junction. The induced charges also lead to the enhancement of the electromagnetic field in the gap between nanoparticles. The field enhancement, R_E , increases with decreasing d_{gap} and can reach extremely high values at bonding plasmon resonances frequencies [68,100]. However, the enhancement at low frequencies, out of resonance, is also considerable, as observed in Fig. 3(c).

When d_{gap} is reduced down to a few Å, the absorption resonances owing to the bonding plasmon modes progressively disappear, and the field enhancement is first saturated and then quenched. This effect is attributed to the establishment of the ac tunneling current across the junction, I_ω , at optical frequencies. The induced charges of opposite sign at the facing metal surfaces are neutralized leading to the observed change of the linear response. Because of the electron transfer through the potential barrier separating the nanoparticles, the lowest (CTP) and higher-energy (CTP') charge transfer plasmon modes emerge. The nanoparticles become conductively coupled prior to the direct geometrical contact between their surfaces. The establishment of I_ω can be identified in Fig. 3(c) for the dimer of Na cylinders. As d_{gap} decreases, the ac current between nanoparticles I_ω first grows exponentially (tunneling regime). Starting from $d_{\text{gap}} \simeq 2$ Å the potential barrier separating the nanoparticles decreases enough so that the electrons close to the Fermi level can move quasi-freely across the junction. In this situation, I_ω is stabilized at a nearly constant value.

Qualitatively, the results obtained for the Al spherical dimer and for the Na nanowires dimer are very similar, except for the relevant frequency and distance ranges. Because of the lower electron density, the dipolar plasmon resonance of an individual Na cylinder is at $\omega = 4$ eV while the dipolar plasmon resonance of an individual Al sphere is at $\omega = 8.7$ eV. As to the relevant distances, the effects of electron tunneling require smaller d_{gap} to be apparent in the Al case. Indeed, the tunneling barrier of the junction is larger in the case of Al because of its higher work function. Note also that because of the much larger radii, the plasmon resonances are better defined for the Na nanowires. In the case of Al, the strong interaction between collective (plasmon) and one-particle electron-hole pair excitations leads to the broadening of the plasmon modes [119]. For the parallel Na slabs (not shown here), the fields in the gap are not enhanced because of the flat geometry. The absorption cross-section in such junction is nearly independent of d_{gap} , and it is characterized by a pronounced resonance at

5.89 eV close to the bulk plasmon frequency, in full agreement with the classical theory [102].

IV. NONLINEAR RESPONSE

A. The role of tunneling

Among the effects influencing the nonlinear response of metal nanostructures, the situations where the incident wave, or the frequency-converted signal (second or third harmonic for example) are in resonance with the plasmon mode of the system have been identified as particularly effective [29–34,48–60]. This resonant effect is illustrated in Fig. 3(d) with the example of an individual Na cylinder in vacuum. The third-order hyperpolarizability, $\alpha^{(3)}(3\omega)$, increases by more than one order of magnitude when the frequency of the third harmonic matches the dipolar plasmon resonance of the individual cylinder, $3\omega = 4$ eV. Similarly, a strong resonant increase of the nonlinear response is also obtained for the dimer, as discussed below in this section.

1. TDDFT results at low frequencies of the fundamental wave

To facilitate the analysis of the different mechanisms involved in the nonlinear response and reveal the effect of electron tunneling across the gap of the nanoantenna, we start our discussion with TDDFT results obtained for the low frequencies of the fundamental wave, as shown in Fig. 4. We use $\omega \leq 1.2$ eV for the Na nanowire dimer and $\omega \leq 2.5$ eV for Al nanospheres, which places the second or third harmonic frequencies below the energies of the plasmon modes of the system (see Fig. 3). The case of the Na nanowire dimer and frequency of the fundamental $\omega = 1.2$ eV is an exception since the third harmonic is in resonance with the red-shifted BDP for well-separated nanowires at $d_{\text{gap}} = 21$ Å. The latter is done on purpose in order to simultaneously illustrate the resonant effect (here at large d_{gap}) and the tunneling contribution (small d_{gap}) to the frequency conversion. It is also noteworthy that considering low frequencies for the incident wave allows for a comparison between the results of the TDDFT calculations and the qualitative analytical trends obtained within the theory of PAT [85–87]. After the contribution of tunneling to the nonlinear response is unveiled, we will extend our analysis to the results obtained at higher frequencies which show resonance effects.

In Fig. 4, we show the enhancement \mathfrak{R} of the nonlinear response due to a dimer configuration. It is defined as the ratio between the intensity of the second ($n = 2$) or third ($n = 3$) harmonic emitted by the dimer and the intensity of the corresponding nonlinear signal obtained from the pair of noninteracting nanoparticles:

$$\mathfrak{R}_n = |p_{n\omega}|^2 / (4|p_{n\omega}^i|^2), \quad (9)$$

where $p_{n\omega}$ is the induced nonlinear dipole of the dimer, and $p_{n\omega}^i$ is the nonlinear dipole of the corresponding individual nanoparticle. Along with the enhancement \mathfrak{R}_n , we also show the scaled ac current through the middle of the junction, $\beta|I_{n\omega}|^2 / (4|p_{n\omega}^i|^2)$, calculated at the second and third harmonic frequency. The scaling parameter β is defined below in this section. Calculations have been performed for the dimer of cylindrical Na nanowires [panel (a)] and for the Al nanosphere

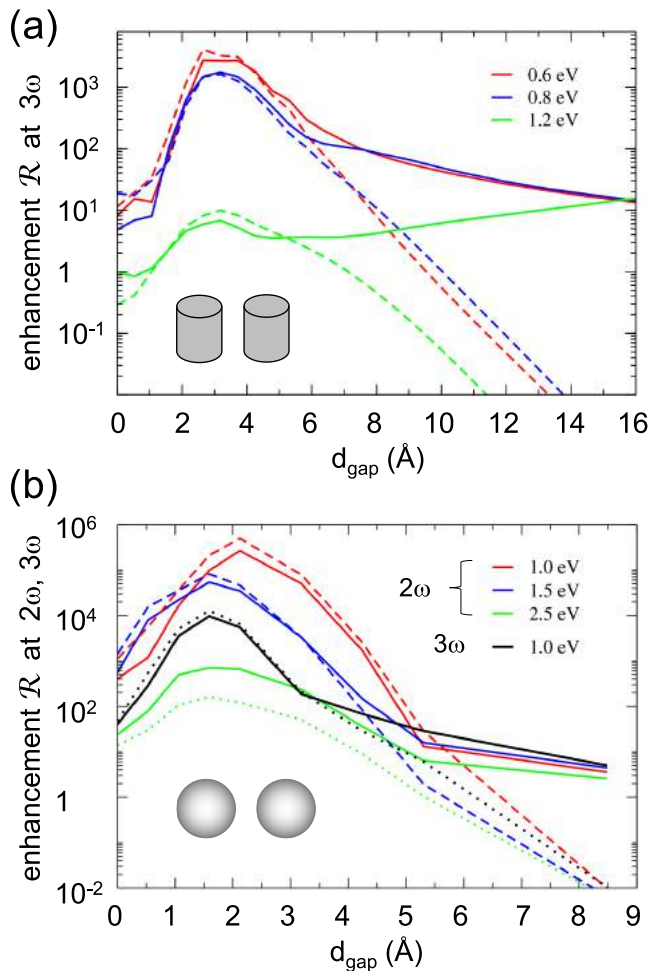


FIG. 4. Nonlinear response of a dimer of (a) cylindrical Na and (b) spherical Al nanoparticles. Results of the TDDFT calculations are shown as a function of the size of the gap between nanoparticles, d_{gap} . Solid lines represent the enhancement of the intensity of the nonlinear dipole $\mathfrak{R}_n = |p_{n\omega}|^2 / (4|p_{n\omega}^i|^2)$ at the second ($n = 2$) and third ($n = 3$) harmonic frequency. Dashed lines represent the scaled ac current through the middle of the junction $\beta |I_{n\omega}|^2 / (4|p_{n\omega}^i|^2)$ calculated at the second and third harmonic frequency. Different colors correspond to results obtained with different frequencies ω of the incident fundamental wave, as detailed in the inserts. For further details see the main text.

dimer [panel (b)]. Results are shown as function of the width of the gap for several frequencies of the incident pulse, as indicated in the inserts.

Overall, the same general trends are obtained for different dimer geometries. The nonlinear conversion is much more efficient for a dimer configuration than for noninteracting nanoparticles with generality, as far as low frequencies ω of the incident electromagnetic wave are used. The intensity of the nonlinear signal progressively increases from large separation distances, as the width of the gap d_{gap} decreases. This increase is due to the field enhancement in the gap of the dimer (see Fig. 3), so that each nanoparticle of the dimer is subjected to a stronger field leading to its larger nonlinear polarization. The TDDFT results obtained here for low ω thus confirm the advantage of using a dimer nanoantenna configuration

as a platform for enhancing nonlinear effects. For slightly larger frequency of the incident wave, $\omega = 1.2$ eV, the dimer of Na cylinders features a qualitatively different behavior with d_{gap} . In this case the third harmonic, $3\omega = 3.6$ eV, is in resonance with the BDP of the dimer at large separation ($d_{\text{gap}} = 21$ Å). Decreasing the width of the gap below this value red shifts the BDP frequency. The resonance condition is lost thereby reducing the nonlinearity, this is despite larger fields are reached for smaller d_{gap} . However, when the width of the gap is further reduced down to the tunneling regime, the third harmonic intensity increases again.

All the TDDFT results for the *nonlinear response* shown in Fig. 4 feature the same trend when the width of the gap is reduced to a few-angstrom range where the electron transport across the junction strongly affects the *linear response* of the system [see Fig. 3(a)]. Namely, the efficiency of the frequency conversion reaches a maximum at $d_{\text{gap}} = 2-3$ Å (depending on the metal) corresponding to the electron transport via an ac tunneling current through the potential barrier separating nanoparticles. For even smaller d_{gap} , when the conductive contact is established across the junction, the conversion efficiency \mathfrak{R}_n drops off by several orders of magnitude. The dimer evolves towards a single, albeit larger, nanoparticle.

At first glance, the main trends in the dependence of the frequency conversion on d_{gap} [Fig. 4(a) and 4(b)] seem to correspond to the gap width dependence of the field enhancement [see Fig. 3(c)]. In particular, the decrease of the nonlinearity for narrow gaps correlates with the quenching of the field enhancement due to the establishment of the optically induced ac current I_{ω} across the junction [see Fig. 3(c)]. It is then tempting to consider that the nonlinear response of the dimer can be explained on the basis of the nonlinear response of the individual nanoparticles subjected to the corresponding enhanced fields. However, a careful inspection of the data obtained for the gap widths of $d_{\text{gap}} < 4-6$ Å shows additional features that might point at a different explanation. (1) The smooth variation of the nonlinearity when decreasing d_{gap} at large separations is replaced by a sharp growth at a separation distance of $d_{\text{gap}} \approx 4-6$ Å, which correlates with the fast increase of the ac electron tunneling across the gap. (2) The change in the behavior of the nonlinear response at $d_{\text{gap}} \approx 4-6$ Å, and the overall dependence of $\mathfrak{R}(d_{\text{gap}})$ in the tunneling region matches the dependence on d_{gap} of the corresponding n th harmonic of the (tunneling) current across the junction, $|I_{n\omega}|^2$, marked with dashed lines for each corresponding case in Figs. 4(a) and 4(b).

In what follows, on a basis of a detailed analysis of the TDDFT results we demonstrate that while for the large d_{gap} the nonlinear response of the dimer is that of individual nanoparticles subjected to enhanced fields, *the electron tunneling, and more generally electron transport through the junction, plays a key role in the formation of the nonlinear response of the dimer structures with narrow gaps* ($d_{\text{gap}} < 4-6$ Å).

2. The nonlinear tunneling currents

Electron tunneling through the junction can influence the nonlinear response due to its effect on the distribution of the fields inside the particles, as well as due to the nonlinearity of the tunneling process itself [67,93–95,120]. The latter can be

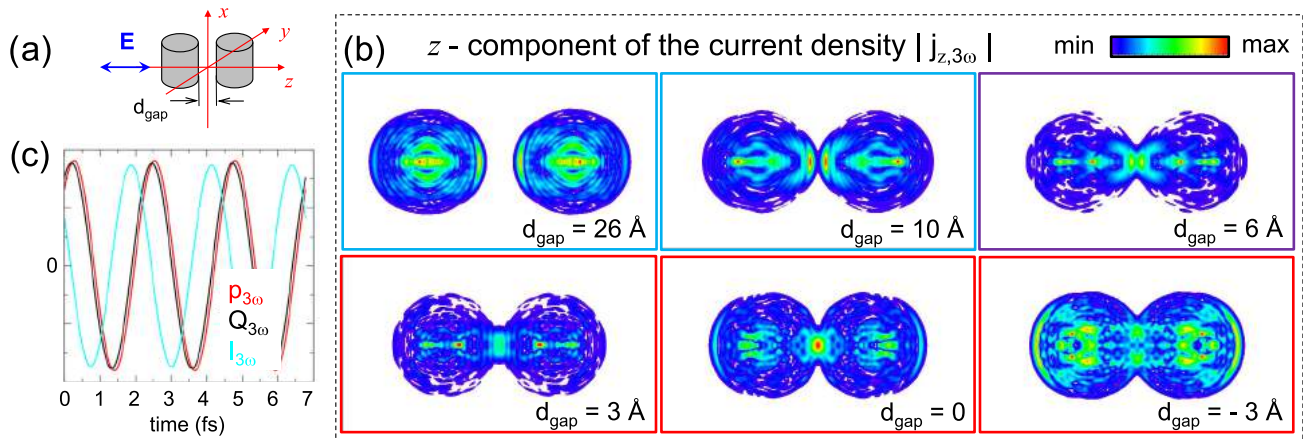


FIG. 5. Analysis of the nonlinear response of the Na cylindrical dimer for the frequency of the fundamental wave $\omega = 0.6$ eV. (a) Sketch of the geometry of the system and of the polarization of the fundamental wave. (b) Color plots of the current density $\hat{j}_{3\omega}$ induced at the third harmonic frequency calculated for several sizes of the gap d_{gap} . The absolute value of the z -component of $\hat{\mathbf{j}}_{3\omega}$, $|j_{z,3\omega}| \equiv |\hat{e}_z \cdot \hat{\mathbf{j}}_{3\omega}|$ is shown in the (y, z) plane perpendicular to the cylinder axis. The color codes are explained in the insert. Blue frames indicate a regime of capacitive coupling between nanoparticles, and red frames indicate a conductive coupling regime. A violet frame is used for an intermediate situation at $d_{\text{gap}} = 6 \text{ \AA}$. (c) Time evolution of the nonlinear dipole $\text{Re}[e^{-i3\omega} p_{3\omega}]$, charge transferred between nanoparticles $\text{Re}[e^{-i3\omega} Q_{3\omega}]$, and current through the junction $\text{Re}[e^{-i3\omega} I_{3\omega}]$ at the third harmonic frequency. Results are shown for $d_{\text{gap}} = 3 \text{ \AA}$, which corresponds to the maximum enhancement of the third harmonic intensity. Here, $\text{Re}[x]$ stands for the real part of x . All the quantities are scaled to 1 at the maximum. The color code is explained in the insert.

qualitatively argued using a semiclassical approach as follows: high harmonics in the tunneling current between nanoparticles, $I_{n\omega}$, arise because of the nonlinearity in the current-voltage characteristic, $I(V)$, of the junction: $I_{n\omega} \propto \frac{\partial^n I}{\partial V^n}(U_{\text{opt}})^n$, where $U_{\text{opt}} = d_{\text{gap}} E_{\omega}^g$ is the optical potential (bias) across the gap [41,82] with E_{ω}^g the corresponding local field in it. Going beyond this simple approach, the quantum theory of photon-assisted tunneling provides a closed-form expression for the time-dependent tunneling current in terms of the complex response function of the junction \mathfrak{J} [85,88]:

$$I(t) = \text{Im} \left[\sum_{n,m} J_n(\alpha) J_{n+m}(\alpha) e^{im\omega t} \mathfrak{J}(V_p + n\omega) \right], \quad (10)$$

where $\text{Im}[x]$ stands for the imaginary part of x , J_k is the Bessel function of order k , and $\alpha = \frac{U_{\text{opt}}}{\omega}$. Assuming that α is small, $J_k(\alpha) \propto \left(\frac{U_{\text{opt}}}{\omega}\right)^k$. Under these conditions, and in agreement with the simple semiclassical approach, it follows from Eq. (10) that the high harmonics in the tunneling current between nanoparticles are given by $I_{n\omega} \propto (d_{\text{gap}} E_{\omega}^g / \omega)^n$. We find that the relative weight of high harmonics in the ac tunneling current through the junction calculated with TDDFT indeed increases as $I_{n\omega} / I_{\omega} \propto (E_{\omega}^g d_{\text{gap}})^{(n-1)}$ with increasing separation between nanoparticles. For the Na cylinder dimer, the $I_{3\omega}$ becomes comparable to the ac tunneling current at the frequency of the fundamental wave I_{ω} at large d_{gap} . Obviously, both tunneling currents are exponentially small in this case.

To further analyze the origin of the nonlinear response, we show in Fig. 5(b) color maps of the absolute value of the z -component of the current density at third harmonic frequency $|j_{z,3\omega}(y, z)|$ for a Na cylindrical dimer nanoantenna, calculated in the (y, z) plane perpendicular to the cylinders axis. The frequency of the fundamental wave is $\omega = 0.6$ eV. Note that because of the strong variation of the nonlinearity with d_{gap}

the color scale is set separately for each panel. Assuming the $\exp(-i\omega t)$ time dependence, the total z -oriented nonlinear dipole per unit length can be obtained from the relationship [118]

$$3\omega p_{3\omega} = i \int dy \int dz j_{z,3\omega}(y, z). \quad (11)$$

Thus the results in Fig. 5 allow one to visualize the relative contributions of the nonlinear currents to $p_{3\omega}$ in the different spatial regions. In particular, we are interested in how the relative weight of the nonlinear tunneling current evolves with d_{gap} .

For well-separated cylinders ($d_{\text{gap}} = 26$ and 10 \AA), the nonlinear current is predominantly excited in the volume of each nanoparticle as well as at the portion of its surface oriented in the direction along the electric field of the incident pulse. Thus we observe the (strong) volume and (weaker) surface contributions to the nonlinear polarization [60]. At these widths of the gap the total dipole $p_{3\omega}$ is built as a sum of the polarizations of individual cylinders. Note that the nonlinear surface currents are the strongest at the surfaces facing the gap because of the field enhancement at the junction. A decrease of the gap width to $d_{\text{gap}} = 10 \text{ \AA}$ leads to larger fields in the gap region so that the contribution of the metal surfaces facing the gap becomes more pronounced.

For $d_{\text{gap}} \leq 8 \text{ \AA}$, the coupling between cylindrical nanowires evolves from capacitive to conductive. In this situation electron tunneling through the junction strongly affects the optical absorption cross section σ as shown in Fig. 3. Along with its effect on the linear response, the electron transport through the junction contributes to the nonlinear polarization of the dimer. Indeed, simultaneously to the presence of the surface currents, the third harmonic current through the junction becomes visible for $d_{\text{gap}} = 6 \text{ \AA}$, and the regions with the strongest

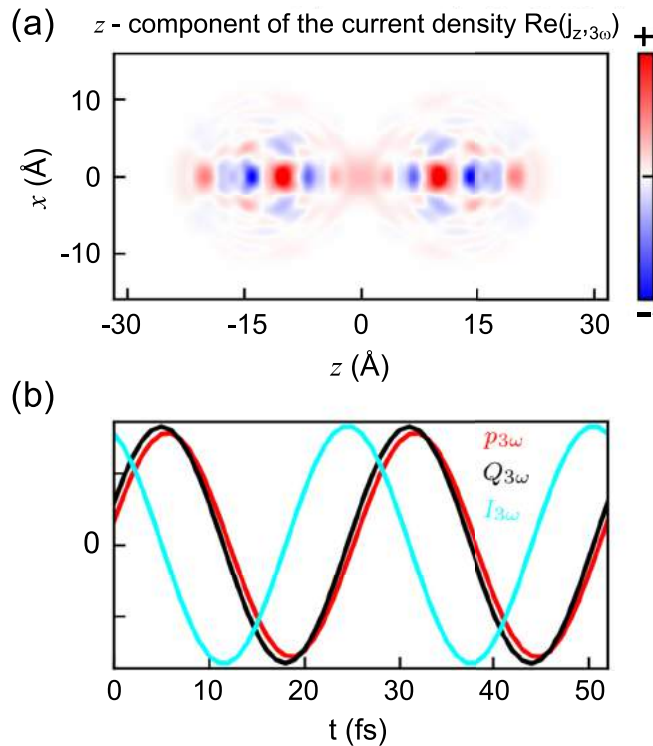


FIG. 6. Analysis of the nonlinear response of an Al spherical dimer for $\omega = 1$ eV. The dimer geometry is characterized by a gap of width $d_{\text{gap}} = 2$ Å, corresponding to the maximum enhancement of the third harmonic intensity. (a) Color plot of the current density $\vec{j}_{3\omega}$ induced at the third harmonic frequency. The real part of the z component of the current density, $\text{Re}(j_{z,3\omega}) \equiv (\hat{e}_z \cdot \vec{j}_{3\omega})$, is shown at the instant of time corresponding to the maximum third harmonic current through the junction. Results are shown in the (x, z) plane with z being the axis of the dimer (see Fig. 1). (b) Time evolution of the nonlinear dipole $\text{Re}[e^{-i3\omega t} p_{3\omega}]$, charge transferred between nanoparticles $\text{Re}[e^{-i3\omega t} Q_{3\omega}]$, and current through the junction $\text{Re}[e^{-i3\omega t} I_{3\omega}]$ at the third harmonic frequency. All the quantities are scaled to 1 at the maximum. The color code is displayed in the insert.

nonlinear current density within the nanoparticle volume shift towards the junction. Note that the volume current density also contains the contribution of the tunneling current. This is because the electrons transferred through the potential barrier of the junction continue to move towards the inner part of the nanoparticle while suffering inelastic scattering and dephasing because of the collisions with the valence electrons [121,122]. Thus it is impossible to explicitly separate the tunneling current contribution to the build up of the total nonlinear polarisation.

A gap width of $d_{\text{gap}} = 3$ Å corresponds to the situation with the strongest enhancement of the nonlinear conversion in the system [see Fig. 4(a)]. In this case, the third harmonic of the tunneling current in the junction region is essential while the surface nonlinear currents are not distinguishable at the scale of the figure.

By further decreasing the width of the gap, at geometrical contact between the cylinders ($d_{\text{gap}} = 0$ Å) the junction becomes metallic. The tunneling barrier for the electrons moving along the dimer axis disappears, the field is expelled outside the junction neck created by the metallic conductive path,

and the field enhancement in the gap is quenched. Interestingly, the nonlinear currents in the gap remain strong relative to the other regions. It is worth stressing however that the total nonlinear polarization and third harmonic currents between nanoparticles are orders (!) of magnitude smaller than that in the tunneling regime at $d_{\text{gap}} = 3$ Å [see Fig. 4(a)]. In this case of conductive contact, we ascribe the strong nonlinear current through the gap region to the system evolution towards the limit of a single elongated peanut-shape nanowire. The formation of the nonlinear dipole involves the charge separation between left and right parts of this compound nanoparticle, which results in electron currents through the junction. Because of the small cross-section of the latter, relatively high currents might be reached. In the fully overlapping geometry ($d_{\text{gap}} = -3$ Å), the role of the nonlinear currents at the bulk of the particles and at the surfaces increases, with the corresponding decrease of the contribution at the junction itself. This is consistent with a recovery of the nonlinear response based on the intrinsic bulk and surface nonlinearity of the full connected system.

3. The nonlinear currents through the junction and build up of the nonlinear response of the dimer

The nonlinear current through the middle of the junction,

$$I_{n\omega} = \iint j_{z,n\omega}(x, y, z = 0) dx dy, \quad (12)$$

transfers a charge $Q_{n\omega} = iI_{n\omega}/(n\omega)$ between the nanoparticles and polarizes the system. Here the relationship $I_{n\omega} = dQ_{n\omega}/dt = -in\omega Q_{n\omega}$ is used assuming harmonic signals. The resulting charge-transfer dipole can be expressed as $DQ_{n\omega} = iDI_{n\omega}/(n\omega)$, with D the (unknown) effective separation between the charges $\pm Q_{n\omega}$ induced in the nanoparticles. In Fig. 5(c), we show the dynamics of the total nonlinear dipole $p_{3\omega}$, the transferred charge $Q_{3\omega}$, and the current $I_{3\omega}$ calculated with TDDFT for the frequency of fundamental wave $\omega = 0.6$ eV, and $d_{\text{gap}} = 3$ Å. These conditions correspond to the maximum enhancement of the third harmonic generation by the dimer nanoantenna. The width of the gap is such that the system is in the tunneling regime, i.e., electron transport through the junction corresponds to the tunneling through the potential barrier between nanoparticles. The total nonlinear dipole evolves in phase with transferred charge and its time evolution is shifted by a quarter of an optical period with respect to that of the current. That is, the dynamics of the total nonlinear dipole is equivalent to that of the charge transfer dipole. This result is consistent with possibly determinant role played by the charge transfer dipole and thus by the electron transport through the junction in the build up of the total nonlinear polarization.

One might consider that for the Na nanowire dimer the increase of nonlinear response for tunneling distances is connected with an effect of proximity of the frequency of the third harmonic to the CTP. For $d_{\text{gap}} = 1-2$ Å, this is indeed the case at low frequencies of the fundamental wave $\omega = 0.6$ and 0.8 eV, and this could further increase the role of the electron transport across the gap. However, the same qualitative results in the behavior of the nonlinear current and the charge transfer are obtained (Fig. 6) in the case of an Al spherical

dimer for the frequency of the fundamental wave $\omega = 1$ eV. In this situation, the third harmonic frequency is well below any resonant excitation in the system [see Fig. 3(b)], which points towards a nonresonant effect, intrinsically associated with the nonlinear tunneling current and therefore supports robustness of our conclusions.

4. Intrinsic versus tunneling contributions

As explained above, the tunneling, volume, and surface components of the total nonlinear current calculated with TDDFT cannot be explicitly separated so that the respective contributions to the nonlinear response cannot be straightforwardly obtained using Eq. (5) or (11). Similarly, the effective separation D between the charges transferred across the junction is *a priori* unknown. To quantify the role of the electron transport through the junction in the nonlinear response, the following procedure can be applied. Let us write the nonlinear dipole of the dimer in the form

$$p_{n\omega} = 2p_{n\omega}^{\text{np}} + p_{n\omega}^{\text{CT}}, \quad (13)$$

where the intrinsic nonlinear polarization of each nanoparticle excluding the effects of nonlinear electron transport through the junction is denoted as $p_{n\omega}^{\text{np}}$, and $p_{n\omega}^{\text{CT}} \equiv iDI_{n\omega}/(n\omega)$ is the nonlinear dipole induced by the nonlinear current between nanoparticles. If the charge-transfer polarization $p_{n\omega}^{\text{CT}}$ provides the main contribution to the total nonlinear dipole, i.e., if $p_{n\omega}^{\text{CT}} \gg p_{n\omega}^{\text{np}}$, then the quantity $\tilde{D} = -in\omega p_{n\omega}^{\text{CT}}/I_{n\omega}$ should be real valued and nearly independent on the width of the gap (we assume $d_{\text{gap}} \ll D$). This is indeed what we obtain from $p_{n\omega}$ and $I_{n\omega}$ calculated with TDDFT at small widths of the gap for both the Na nanowire (below 6 Å) and for the Al nanosphere dimer (below 4 Å). Thus, \tilde{D} can be used to find an effective separation $D = \text{Re}[\tilde{D}]$ between the charges induced at the nanoparticles at the corresponding n th harmonic frequency because of the electron transport across the junction.

We find that for the Al nanosphere dimer the effective separation D is very close to $2R_{\text{sph}}$ for both the second and third harmonic cases. The transferred charge is effectively located close to the center of the nanoparticles as one would expect considering the symmetry and small size of the Al spheres. For the Na nanowire dimer, because of the relatively large cylinder radii, the nonlocal screening effects become important. Depending on the frequency, we find an effective separation distance D within 15–50 Å, i.e., $D < 2R_{\text{cyl}}$. For all the systems, at large widths of the gap, the quantity \tilde{D} diverges. This is because the tunneling current $I_{n\omega}$ becomes exponentially small in such a situation, and the intrinsic polarization $p_{n\omega}^{\text{np}}$ of each particle provides the leading contribution to the total nonlinear dipole.

With parameter D as defined above, and fixed to its value at small width of the junction, we can estimate the frequency conversion enhancement \mathfrak{X} owing exclusively to the charge-transfer dipole $p_{n\omega}^{\text{CT}}$. It is given by $\mathfrak{X} = \beta|I_{n\omega}|^2/4|p_{n\omega}^{\text{CT}}|^2$, where $\beta = (D/n\omega)^2$. The charge transfer contribution \mathfrak{X} is shown in Figs. 4(a) and 4(b) with dashed lines. In the range of the gap widths where the electron transfer across the gap is efficient, the agreement between the TDDFT result shown in Fig. 4 with solid lines and the prediction obtained by considering only the charge transfer between cylinders is remarkable. This

points at the dominant role of the nonlinear currents in the gap as responsible for the frequency conversion by the dimer. In particular, as follows from Figs. 3(c) and 4, the maximum of the frequency conversion is reached in the tunneling regime, prior to the establishment of the conductive contact between nanoparticles with possibility of the ballistic electron transport through the junction.

The results in Fig. 4 also nicely visualize the transition between “tunneling” and “intrinsic” regimes of the nonlinearity with increasing d_{gap} . As the width of the junction increases, and the tunneling effects become exponentially low, the \mathfrak{X} dependence on d_{gap} changes to a much smoother variation (solid lines). At these large widths of the gap, the total nonlinear dipole is built by intrinsic polarizations of the nanoparticles which is determined by the field enhancement in the system and decreases with increasing d_{gap} . A departure from this general behavior at large distances can be observed for the Na cylinder dimer, at $\omega = 1.2$ eV, where \mathfrak{X} grows with d_{gap} . However, this is due to the spectral overlap with the BDP resonance of the dimer, which approaches the third harmonic frequency in this particular case.

It is noteworthy that an efficient generation of the second and third harmonics in the tunneling current and thus the build up of the nonlinear dipole due to the charge transferred between nanoparticles is possible in the spherical and cylindrical dimer configurations owing to the field enhancement in the junction. As follows from Eq. (10), the harmonics in the tunneling current between nanoparticles $I_{n\omega}$ are determined by the enhanced fields in the junction $I_{n\omega} \propto (E_{\omega}^{\text{g}})^n$. In this respect, $I_{n\omega}$ should be more sensitive to the field enhancement than the intrinsic polarization representing the integral over the nanoparticle volume. The TDDFT calculations performed for the parallel metallic slabs further support the conclusion on the importance of the field enhancement in the gap. Despite the presence of nonlinear tunneling currents in this case, we do not observe any enhancement of the nonlinearity when decreasing d_{gap} . This result is consistent with the absence of the field enhancement in the vacuum gap between flat metal surfaces.

B. Role of resonant plasmonic modes

While a dimer nanoantenna generally enables a more efficient frequency conversion as compared to the corresponding independent nanoparticles, this “rule of thumb” is subject to specific conditions determined by the width of the junction, and by the respective role of the electron transport across the gap and of the plasmon modes of the nanoantenna. Depending on whether one seeks the strongest gain of the nonlinearity as compared to the single nanoparticle (relative efficiency), or the largest intensity of the nonlinear signal (absolute efficiency), the choice of the dimer structure might differ, as revealed by the TDDFT results shown in Fig. 7. The third harmonic generation in the Na cylinder dimer is analyzed in this figure for a wide range of gap widths and different frequencies ω of the incident fundamental wave. The main difference between the two panels in Fig. 7 is that Fig. 7(a) shows the effect of the collective response of the dimer relative to the independent individual nanoparticles, while Fig. 7(b) provides the information on the absolute value of the nonlinear response.

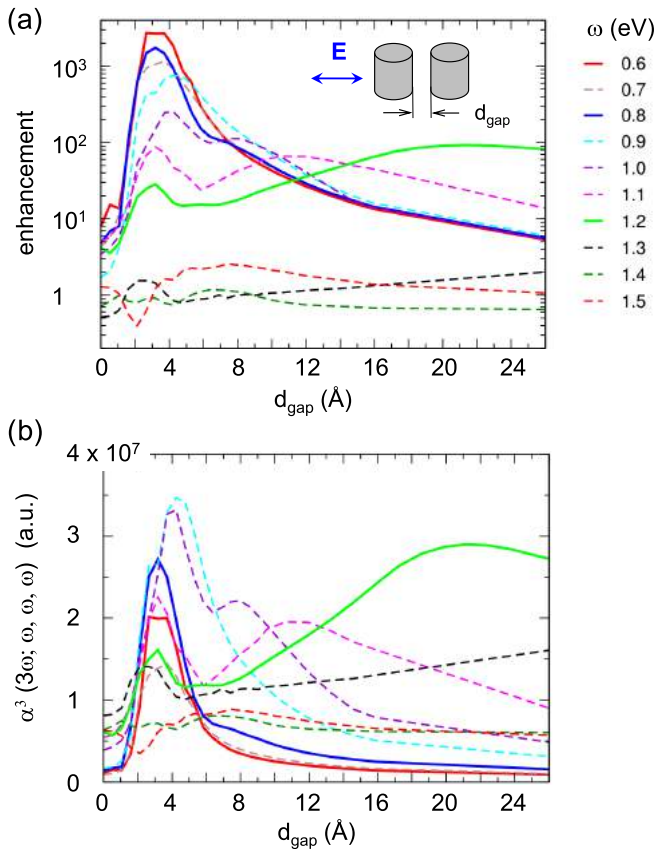


FIG. 7. Third harmonic generation in a Na cylinder dimer. The polarization of the incident plane wave is sketched in the insert of (a). TDDFT results are presented as a function of the size of the gap between nanoparticles d_{gap} . (a) Enhancement of the intensity of the emitted third harmonic, \mathfrak{R} , as compared to the case of the individual noninteracting nanoparticles. For the exact definition of \mathfrak{R} see Eq. (9). (b) Hyperpolarizability, $\alpha^{(3)}(3\omega)$, of the same dimer. The values are given in atomic units (a.u.). The relation $1 \text{ esu} = 0.1985 \times 10^{40} \text{ a.u.}$ can be used for conversion to electrostatic units (esu). Different colors correspond to results obtained with different frequencies ω of the incident fundamental wave, as detailed in the insert of (a).

We start our discussion with the dependence of the enhancement of the intensity of the emitted third harmonic, \mathfrak{R} , on the width of the junction [Fig. 7(a)]. The largest enhancement (nearly four orders of magnitude) is reached at low frequencies of the fundamental wave in the tunneling regime (tunneling enhancement, TE, in narrow gaps) because of the nonlinear electron transport across the gap. As the frequency of the incident fundamental wave is increased, the gain in the third harmonic intensity because of the dimer structure as compared to the two individual noninteracting nanoparticles becomes smaller. This is because of (i) the overall decrease in the nonlinearity of tunneling current [see Eq. (10)] and (ii) the enhancement of the third harmonic intensity from the single nanoparticle since 3ω approaches its dipolar plasmon resonance (see Fig. 3). For the frequencies of the fundamental wave ω above 1.2 eV, no noticeable effect of the tunneling enhancement can be observed.

Together with the main maximum of the nonlinear enhancement in the tunneling regime at $d_{\text{gap}} = 3\text{--}4 \text{ \AA}$, the results

obtained for larger frequencies of the fundamental wave, at $\omega = 0.9, 1.0, 1.1,$ and 1.2 eV also show an additional, weaker, feature at larger d_{gap} . This corresponds to a resonant process [resonant enhancement, RE]. At these frequencies of the fundamental wave, the corresponding third harmonic frequency is below the dipolar plasmon mode of the individual cylinder [see Fig. 3(d)]. However, the plasmon coupling [101] in a dimer configuration redshifts the dipolar plasmon frequency so that at a given d_{gap} the third harmonic can be at resonance with the BDP plasmon mode of the dimer. This leads to the RE of the nonlinear polarization. The redshift of the BDP frequency with decreasing d_{gap} translates into the corresponding shift of the RE maximum, which appears at smaller d_{gap} when decreasing ω .

At frequencies of the fundamental wave $\omega = 1.3, 1.4,$ and 1.5 eV , the third harmonic spans the high frequency wing of the RE for the individual cylinder owing to the dipolar plasmon mode [see Fig. 3(d)]. Since the dimer configuration redshifts the BDP out of resonance and because of the relatively small TE at high frequencies, \mathfrak{R} decreases by several orders of magnitude. It reaches values close to unity, i.e., the dimer performs equally good as the noninteracting cylinders in these circumstances. This is despite the fact that the field enhancement in the gap between nanoparticles *a priori* should increase the nonlinear response, however, the resonance effects outperform the effects of the field enhancement.

Thus, at low frequency of the fundamental wave, the field enhancement and tunneling effects in the gap between nanoparticles result in the strongest gain of the frequency conversion obtained with a dimer, as compared to individual nanoparticles. At the same time, reaching the maximum absolute value of the nonlinear response might not necessarily require the same conditions, as follows from Fig. 7(b). In this figure, the TDDFT results for the hyperpolarizability, $\alpha^{(3)}(3\omega)$, of the dimer are shown as a function of the width of the junction for different frequencies of the fundamental wave. The maximum value of $\alpha^{(3)}(3\omega)$ is obtained for a narrow junction, not at the lowest frequencies but at an intermediate frequency range between $\omega = 0.9$ and 1.0 eV , where tunneling and resonance effects overlap. Comparable high nonlinear hyperpolarizability is obtained at $\omega = 1.2 \text{ eV}$ for a wide gap of $d_{\text{gap}} = 21 \text{ \AA}$, where the third harmonic frequency is at resonance with the BDP plasmon mode of the dimer. At even higher frequencies, the hyperpolarizability $\alpha^{(3)}(3\omega)$ shows only mild variations with d_{gap} and its frequency dependence is mainly determined by the plasmon resonance of the individual cylinders.

One remark is in order before closing this section. We intentionally did not perform calculations with higher frequencies of the fundamental wave in resonance with the plasmon modes of the system. While this situation is known to provide strong enhancement of the nonlinearity [5,30,43,47,48,52,60,61], the nonlinear tunneling effects would be small at these relatively high frequencies, and thus difficult to reveal. Moreover, since the incident pulse needed to observe nonlinear effects is intense, a frequency match with the plasmon resonance in the absorption cross section would result in strong electron emission. Precisely, this efficient conversion of the optical energy into electron-hole pairs via an intermediate plasmon excitation has made plasmonics a very attractive tool for solar energy harvesting or for photochemical applications [123–129].

However, in the present case, hot electron emission would result in a spread of the electron density over the entire computational grid, leading to the loss of precision.

V. SUMMARY AND CONCLUSIONS

In summary, using quantum calculations based on the time dependent density functional theory, we obtained the nonlinear response in plasmonic free-electron-metal dimer nanoantennas with narrow gaps. The analysis of the real-time dynamics of the electron density in response to an incident intense electromagnetic pulse, allowed us to elucidate the role of the nonlinear quantum tunneling and plasmon resonances in the second and third harmonic generation from these systems.

We found that depending on the main contributions to the nonlinear response, three interaction regimes can be identified in a dimer nanoantenna.

(i) At large widths of the gap between nanoparticles, $d_{\text{gap}} > 6\text{--}8 \text{ \AA}$ (separated nanoparticles), the total nonlinear polarization of the dimer is given by the sum of the nonlinear polarizations of individual nanoparticles. The coupling between the nanoparticles in the dimer, and, in particular, the field enhancement in the gap increases in overall the nonlinear response.

(ii) In the tunneling distance range of $2 \text{ \AA} < d_{\text{gap}} < 6\text{--}8 \text{ \AA}$, the harmonic components of the ac electron tunneling current through the gap between nanoparticles build the nonlinear charge-transfer dipole. Along with the response of the individual nanoparticles, this charge-transfer dipole contributes to the total nonlinear polarization of the dimer. At low frequencies (0.6–1.5 eV depending on the metal) of the fundamental incident wave, the nonlinear tunneling current across the junction determines and governs the nonlinear response of the dimer. It might lead to orders of magnitude increase of the frequency conversion.

(iii) Finally, for a situation of geometrical overlap between nanoparticle surfaces, a conductive contact is established. The nonlinear response of the dimer evolves to that of a single nanoparticle, albeit of larger size. The strong gap-induced enhancement of the nonlinear signal is quenched in this situation, consistent with experimental observations [42,72].

The three ranges of gap widths pointed out above are defined with respect to the transport properties of the junction. In that respect, they are very similar to the definition proposed earlier, based on the quantum effects in the linear response [130].

It is worth to stress that the incident field enhancement in the gap of the dimer structure is at the origin of the strong

nonlinear effects due to both the nonlinear polarizations of individual nanoparticles and the nonlinear electron tunneling mechanisms. In the former case, it leads to the overall increase of the fundamental field seen by each nanoparticle, while in the latter case it results in the high optical bias across the junction producing the strong nonlinear current between nanoparticles.

Along with the tunneling enhancement mechanism, our TDDFT calculations confirm a pronounced resonance enhancement of the nonlinear response when the second or third harmonic frequency matches the plasmon mode of the dimer. This effect was also reported in earlier studies [5,30,42,53,54]. We concluded that if one seeks the best performance of the dimer compared to the noninteracting nanoparticles, the low-frequency range and the tunneling regime might provide an appropriate solution. At the same time, if the largest absolute value of the emitted harmonic is sought, either using the tunneling regime at small gap width, or setting the emission frequency in resonance with the bonding plasmon mode at large gap width, can be equally efficient.

Finally, the present work enabled the theoretical study of the mechanisms involved in the generation of the harmonics of the fundamental frequency in the dimer nanoantennas with subnanometer gaps, a very challenging regime. The TDDFT approach goes beyond hydrodynamic treatments of the nonlinear response [60,90–92], since it naturally accounts for electron tunneling. Thus the role of the nonlinear tunneling currents addressed previously using parameterized classical or semiclassical approaches [93–95] has been demonstrated here on full-quantum grounds. While our work addresses small-size plasmonic nanoparticles, the demonstration of the effect of nonlinear tunneling currents is of relevance for larger systems with narrow gaps. Considering the current experimental capabilities to build plasmonic junctions that reach atomic scale [40–42,49,71–77,82–84], we believe that the understanding of the mechanisms of the nonlinear response in narrow gaps is of paramount importance for designing of efficient nonlinear nanoscale devices giving rise to a broad range of optoelectronic applications.

ACKNOWLEDGMENTS

G.A., R.E., and J.A. acknowledge the projects FIS2016-80174-P from Spanish MINECO, project 70NANB15H32 from U.S. Department of Commerce, National Institute of Standards and Technology. G.A., R.E., and A.K.K. acknowledge project PI2017-30 of the Department of Education of the Basque Government.

-
- [1] R. M. Osgood, N. C. Panoiu, J. I. Dadap, X. Liu, X. Chen, I.-W. Hsieh, E. Dulkeith, W. M. Green, and Y. A. Vlasov, *Adv. Opt. Photon.* **1**, 162 (2009).
 - [2] D. Smirnova and Y. S. Kivshar, *Optica* **3**, 1241 (2016).
 - [3] N. I. Zheludev, *Contemp. Phys.* **43**, 365 (2002).
 - [4] N. I. Zheludev and Y. S. Kivshar, *Nat. Mater.* **11**, 917 (2012).
 - [5] M. Kauranen and A. V. Zayats, *Nat. Photonics* **6**, 737 (2012).
 - [6] J. E. Sharping, K. F. Lee, M. A. Foster, A. C. Turner, B. S. Schmidt, M. Lipson, A. L. Gaeta, and P. Kumar, *Opt. Express* **14**, 12388 (2006).
 - [7] M. A. Foster, A. C. Turner, M. Lipson, and A. L. Gaeta, *Opt. Express* **16**, 1300 (2008).
 - [8] M. Schultze, E. M. Bothschafter, A. Sommer, S. Holzner, W. Schweinberger, M. Fiess, M. Hofstetter, R. Kienberger, V. Apalkov, V. S. Yakovlev, M. I. Stockman, and F. Krausz, *Nature* **493**, 75 (2013).
 - [9] C. Argyropoulos, P.-Y. Chen, F. Monticone, G. D’Aguanno, and A. Alù, *Phys. Rev. Lett.* **108**, 263905 (2012).
 - [10] V. J. Sorger, R. F. Oulton, R.-M. Ma, and X. Zhang, *MRS Bull.* **37**, 728 (2012).

- [11] A. Zoumi, A. Yeh, and B. J. Tromberg, *Proc. Natl. Acad. Sci. U.S.A.* **99**, 11014 (2002).
- [12] P. J. Campagnola, A. C. Millard, M. Terasaki, P. E. Hoppe, C. J. Malone, and W. A. Mohler, *Biophys. J.* **82**, 493 (2002).
- [13] V. Kravtsov, R. Ulbricht, J. M. Atkin, and M. B. Raschke, *Nat. Nano* **11**, 459 (2016).
- [14] A. Horneber, K. Braun, J. Rogalski, P. Leiderer, A. J. Meixner, and D. Zhang, *Phys. Chem. Chem. Phys.* **17**, 21288 (2015).
- [15] R. M. Corn and D. A. Higgins, *Chem. Rev.* **94**, 107 (1994).
- [16] J. Butet and O. J. F. Martin, *ACS Nano* **8**, 4931 (2014).
- [17] A. Hohenau, J. R. Krenn, J. Beermann, S. I. Bozhevolnyi, S. G. Rodrigo, L. Martin-Moreno, and F. Garcia-Vidal, *Phys. Rev. B* **73**, 155404 (2006).
- [18] M. Mesch, B. Metzger, M. Hentschel, and H. Giessen, *Nano Lett.* **16**, 3155 (2016).
- [19] M. Lewenstein, P. Balcou, M. Y. Ivanov, A. L'Huillier, and P. B. Corkum, *Phys. Rev. A* **49**, 2117 (1994).
- [20] F. Krausz and M. Ivanov, *Rev. Mod. Phys.* **81**, 163 (2009).
- [21] L. Gallmann, C. Cirelli, and U. Keller, *Annu. Rev. Phys. Chem.* **63**, 447 (2012).
- [22] G. A. Wurtz and A. V. Zayats, *Laser Photon. Rev.* **2**, 125 (2008).
- [23] K. F. MacDonald, Z. L. Sámson, M. I. Stockman, and N. I. Zheludev, *Nat. Photonics* **3**, 55 (2009).
- [24] H. Husu, R. Siikanen, J. Mäkitalo, J. Lehtolahti, J. Laukkanen, M. Kuittinen, and M. Kauranen, *Nano Lett.* **12**, 673 (2012).
- [25] J. Y. Suh and T. W. Odom, *Nano Today* **8**, 469 (2013).
- [26] M. Castro-Lopez, D. Brinks, R. Sapienza, and N. F. van Hulst, *Nano Lett.* **11**, 4674 (2011).
- [27] P.-Y. Chen, C. Argyropoulos, and A. Alù, *Nanophotonics* **1**, 221 (2012).
- [28] G. Grinblat, M. Rahmani, E. Cortés, M. Caldarola, D. Comedi, S. A. Maier, and A. V. Bragas, *Nano Lett.* **14**, 6660 (2014).
- [29] T. Hanke, G. Krauss, D. Träutlein, B. Wild, R. Bratschitsch, and A. Leitenstorfer, *Phys. Rev. Lett.* **103**, 257404 (2009).
- [30] J. Butet, P.-F. Brevet, and O. J. F. Martin, *ACS Nano* **9**, 10545 (2015).
- [31] M. Lippitz, M. A. van Dijk, and M. Orrit, *Nano Lett.* **5**, 799 (2005).
- [32] R. Czapllicki, J. Mäkitalo, R. Siikanen, H. Husu, J. Lehtolahti, M. Kuittinen, and M. Kauranen, *Nano Lett.* **15**, 530 (2015).
- [33] B. Metzger, M. Hentschel, and H. Giessen, *Nano Lett.* **17**, 1931 (2017).
- [34] Y. Zhang, A. Manjavacas, N. J. Hogan, L. Zhou, C. Ayala-Orozco, L. Dong, J. K. Day, P. Nordlander, and N. J. Halas, *Nano Lett.* **16**, 3373 (2016).
- [35] A. V. Gorbach, *Phys. Rev. A* **87**, 013830 (2013).
- [36] J. D. Cox and F. J. G. d. Abajo, *Nat. Commun.* **5**, 5725 (2014).
- [37] H. Rostami, M. I. Katsnelson, and M. Polini, *Phys. Rev. B* **95**, 035416 (2017).
- [38] W. Cai, A. P. Vasudev, and M. L. Brongersma, *Science* **333**, 1720 (2011).
- [39] D. de Ceglia, M. A. Vincenti, and M. Scalora, *J. Opt.* **18**, 115002 (2016).
- [40] A. Bouhelier, M. Beversluis, A. Hartschuh, and L. Novotny, *Phys. Rev. Lett.* **90**, 013903 (2003).
- [41] A. Stolz, J. Berthelot, M.-M. Mennemanteuil, G. C. des Francs, L. Markey, V. Meunier, and A. Bouhelier, *Nano Lett.* **14**, 2330 (2014).
- [42] M. Danckwerts and L. Novotny, *Phys. Rev. Lett.* **98**, 026104 (2007).
- [43] H. Harutyunyan, G. Volpe, R. Quidant, and L. Novotny, *Phys. Rev. Lett.* **108**, 217403 (2012).
- [44] H. Aouani, M. Rahmani, M. Navarro-Cía, and S. A. Maier, *Nat. Nanotechnol.* **9**, 290 (2014).
- [45] J. Berthelot, G. Bachelier, M. Song, P. Rai, G. C. des Francs, A. Dereux, and A. Bouhelier, *Opt. Express* **20**, 10498 (2012).
- [46] L.-J. Black, P. R. Wiecha, Y. Wang, C. H. de Groot, V. Paillard, C. Girard, O. L. Muskens, and A. Arbouet, *ACS Photonics* **2**, 1592 (2015).
- [47] H. Aouani, M. Navarro-Cía, M. Rahmani, T. P. H. Sidiropoulos, M. Hong, R. F. Oulton, and S. A. Maier, *Nano Lett.* **12**, 4997 (2012).
- [48] K. Thyagarajan, S. Rivier, A. Lovera, and O. J. Martin, *Opt. Express* **20**, 12860 (2012).
- [49] J. B. Lassiter, X. Chen, X. Liu, C. Ciraci, T. B. Hoang, S. Larouche, S.-H. Oh, M. H. Mikkelsen, and D. R. Smith, *ACS Photonics* **1**, 1212 (2014).
- [50] M. S. Nezami, D. Yoo, G. Hajisalem, S.-H. Oh, and R. Gordon, *ACS Photonics* **3**, 1461 (2016).
- [51] M. Celebrano, X. Wu, M. Baselli, S. Großmann, P. Biagioni, A. Locatelli, C. De Angelis, G. Cerullo, R. Osellame, B. Hecht, L. Duò, F. Ciccacci, and M. Finazzi, *Nat. Nano* **10**, 412 (2015).
- [52] M. Hentschel, T. Utikal, H. Giessen, and M. Lippitz, *Nano Lett.* **12**, 3778 (2012).
- [53] A. Slablab, L. L. Xuan, M. Zielinski, Y. de Wilde, V. Jacques, D. Chauvat, and J.-F. Roch, *Opt. Express* **20**, 220 (2012).
- [54] J. Butet, S. Dutta-Gupta, and O. J. F. Martin, *Phys. Rev. B* **89**, 245449 (2014).
- [55] S. V. Fomichev, S. V. Popruzhenko, D. F. Zaretsky, and W. Becker, *J. Phys. B* **36**, 3817 (2003).
- [56] B. Metzger, T. Schumacher, M. Hentschel, M. Lippitz, and H. Giessen, *ACS Photonics* **1**, 471 (2014).
- [57] M. Ethis de Corny, N. Chauvet, G. Laurent, M. Jeannin, L. Olgeirsson, A. Drezet, S. Huant, G. Dantelle, G. Nogues, and G. Bachelier, *ACS Photonics* **3**, 1840 (2016).
- [58] K. Uchida, S. Kaneko, S. Omi, C. Hata, H. Tanji, Y. Asahara, A. J. Ikushima, T. Tokizaki, and A. Nakamura, *J. Opt. Soc. Am. B* **11**, 1236 (1994).
- [59] T.-M. Liu, S.-P. Tai, C.-H. Yu, Y.-C. Wen, S.-W. Chu, L.-J. Chen, M. R. Prasad, K.-J. Lin, and C.-K. Sun, *Appl. Phys. Lett.* **89**, 043122 (2006).
- [60] P. Ginzburg, A. V. Krasavin, G. A. Wurtz, and A. V. Zayats, *ACS Photonics* **2**, 8 (2015).
- [61] J. Hurst, F. Haas, G. Manfredi, and P.-A. Hervieux, *Phys. Rev. B* **89**, 161111 (2014).
- [62] C. Ciraci, R. T. Hill, J. J. Mock, Y. Urzhumov, A. I. Fernández-Domínguez, S. A. Maier, J. B. Pendry, A. Chilkoti, and D. R. Smith, *Science* **337**, 1072 (2012).
- [63] G. Toscano, S. Raza, A.-P. Jauho, N. A. Mortensen, and M. Wubs, *Opt. Express* **20**, 4176 (2012).
- [64] F. J. García de Abajo, *J. Phys. Chem. C* **112**, 17983 (2008).
- [65] A. I. Fernández-Domínguez, A. Wiener, F. J. García-Vidal, S. A. Maier, and J. B. Pendry, *Phys. Rev. Lett.* **108**, 106802 (2012).
- [66] J. Zuloaga, E. Prodan, and P. Nordlander, *Nano Lett.* **9**, 887 (2009).
- [67] D. Marinica, A. Kazansky, P. Nordlander, J. Aizpurua, and A. G. Borisov, *Nano Lett.* **12**, 1333 (2012).
- [68] T. V. Teperik, P. Nordlander, J. Aizpurua, and A. G. Borisov, *Opt. Express* **21**, 27306 (2013).

- [69] A. Varas, P. García-González, J. Feist, F. J. García-Vidal, and A. Rubio, *Nanophotonics* **5**, 409 (2016).
- [70] P. Zhang, J. Feist, A. Rubio, P. García-González, and F. J. García-Vidal, *Phys. Rev. B* **90**, 161407 (2014).
- [71] J. A. Scholl, A. García-Etxarri, A. L. Koh, and J. A. Dionne, *Nano Lett.* **13**, 564 (2013).
- [72] G. Hajisalem, M. S. Nezami, and R. Gordon, *Nano Lett.* **14**, 6651 (2014).
- [73] W. Zhu and K. B. Crozier, *Nat. Commun.* **5**, 5228 (2014).
- [74] K. J. Savage, M. M. Hawkeye, R. Esteban, A. G. Borisov, J. Aizpurua, and J. J. Baumberg, *Nature (London)* **491**, 574 (2012).
- [75] H. Jung, H. Cha, D. Lee, and S. Yoon, *ACS Nano* **9**, 12292 (2015).
- [76] H. Cha, J. H. Yoon, and S. Yoon, *ACS Nano* **8**, 8554 (2014).
- [77] D. Xiang, J. Wu, and R. Gordon, *Nano Lett.* **17**, 2584 (2017).
- [78] J. K. Gimzewski, B. Reihl, J. H. Coombs, and R. R. Schlittler, *Z. Phys. B* **72**, 497 (1988).
- [79] R. Berndt, J. K. Gimzewski, and P. Johansson, *Phys. Rev. Lett.* **67**, 3796 (1991).
- [80] J. Kern, R. Kulllock, J. Prangma, M. Emmerling, M. Kamp, and B. Hecht, *Nat. Photonics* **9**, 582 (2015).
- [81] W. Du, T. Wang, H.-S. Chu, and C. A. Nijhuis, *Nat. Photonics* **11**, 623 (2017).
- [82] D. R. Ward, F. Hüser, F. Pauly, J. C. Cuevas, and D. Natelson, *Nat. Nanotechnol.* **5**, 732 (2010).
- [83] R. Arielly, A. Ofarim, G. Noy, and Y. Selzer, *Nano Lett.* **11**, 2968 (2011).
- [84] M. Lenner, P. Rácz, P. Dombi, G. Farkas, and N. Kroó, *Phys. Rev. B* **83**, 205428 (2011).
- [85] J. R. Tucker and M. J. Feldman, *Rev. Mod. Phys.* **57**, 1055 (1985).
- [86] M. Grifoni and P. Hänggi, *Phys. Rep.* **304**, 229 (1998).
- [87] G. Platero and R. Aguado, *Phys. Rep.* **395**, 1 (2004).
- [88] M. H. Pedersen and M. Büttiker, *Phys. Rev. B* **58**, 12993 (1998).
- [89] I. Urdaneta, A. Keller, O. Atabek, and V. Mujica, *J. Chem. Phys.* **127**, 154110 (2007).
- [90] N. Crouseilles, P.-A. Hervieux, and G. Manfredi, *Phys. Rev. B* **78**, 155412 (2008).
- [91] C. Ciraci, M. Scalora, and D. R. Smith, *Phys. Rev. B* **91**, 205403 (2015).
- [92] A. V. Krasavin, P. Ginzburg, G. A. Wurtz, and A. V. Zayats, *Nat. Commun.* **7**, 11497 (2016).
- [93] J. W. Haus, D. de Ceglia, M. A. Vincenti, and M. Scalora, *J. Opt. Soc. Am. B* **31**, A13 (2014).
- [94] M. Scalora, M. A. Vincenti, D. de Ceglia, and J. W. Haus, *Phys. Rev. A* **90**, 013831 (2014).
- [95] P.-Y. Chen, K. Q. Le, and A. Alù, *MRS Commun.* **5**, 565 (2015).
- [96] P.-Y. Chen, R. Salas, and M. Farhat, *J. Opt.* **19**, 124012 (2017).
- [97] M. A. L. Marques and E. K. U. Gross, *Annu. Rev. Phys. Chem.* **55**, 427 (2004).
- [98] R. E. Stratmann, G. E. Scuseria, and M. J. Frisch, *J. Chem. Phys.* **109**, 8218 (1998).
- [99] T. Fennel, K.-H. Meiwes-Broer, J. Tiggesbäumker, P.-G. Reinhard, P. M. Dinh, and E. Suraud, *Rev. Mod. Phys.* **82**, 1793 (2010).
- [100] I. Romero, J. Aizpurua, G. W. Bryant, and F. J. G. de Abajo, *Opt. Express* **14**, 9988 (2006).
- [101] N. J. Halas, S. Lal, W.-S. Chang, S. Link, and P. Nordlander, *Chem. Rev.* **111**, 3913 (2011).
- [102] E. N. Economou, *Phys. Rev.* **182**, 539 (1969).
- [103] N. D. Lang and W. Kohn, *Phys. Rev. B* **3**, 1215 (1971).
- [104] W. A. de Heer, *Rev. Mod. Phys.* **65**, 611 (1993).
- [105] W. A. de Heer, P. Milani, and A. Chatelain, *Phys. Rev. Lett.* **63**, 2834 (1989).
- [106] T. Fennel, G. F. Bertsch, and K.-H. Meiwes-Broer, *Eur. Phys. J. D* **29**, 367 (2004).
- [107] A. Liebsch and W. L. Schaich, *Phys. Rev. B* **40**, 5401 (1989).
- [108] M. W. Knight, N. S. King, L. Liu, H. O. Everitt, P. Nordlander, and N. J. Halas, *ACS Nano* **8**, 834 (2013).
- [109] G. Maidecchi, G. Gonella, R. Proietti Zaccaria, R. Moroni, L. Anghinolfi, A. Giglia, S. Nannarone, L. Mattered, H.-L. Dai, and M. Canepa, *ACS Nano* **7**, 5834 (2013).
- [110] W. Kohn and S. L. J., *Phys. Rev.* **140**, A1133 (1965).
- [111] D. C. Marinica *et al.*, *Sci. Adv.* **1**, e1501095 (2015).
- [112] M. D. Feit, J. A. Fleck, and A. Steiger, *J. Comput. Phys.* **47**, 412 (1982).
- [113] D. Kosloff and R. Kosloff, *J. Comput. Phys.* **52**, 35 (1983).
- [114] O. Gunnarsson and B. I. Lundqvist, *Phys. Rev. B* **13**, 4274 (1976).
- [115] C. H. Lee, R. K. Chang, and N. Bloembergen, *Phys. Rev. Lett.* **18**, 167 (1967).
- [116] O. A. Aktsipetrov, A. A. Fedyanin, E. D. Mishina, A. N. Rubtsov, C. W. van Hasselt, M. A. C. Devillers, and T. Rasing, *Phys. Rev. B* **54**, 1825 (1996).
- [117] G. Aguirregabiria, D. C. Marinica, R. Esteban, A. K. Kazansky, J. Aizpurua, and A. G. Borisov, *ACS Photonics* **4**, 613 (2017).
- [118] J. D. Jackson, *Classical Electrodynamics*, 3rd ed. (Wiley, NY, 1999).
- [119] E. Prodan, P. Nordlander, and N. J. Halas, *Nano Lett.* **3**, 1411 (2003).
- [120] J. W. Haus, D. de Ceglia, M. A. Vincenti, and M. Scalora, *J. Opt. Soc. Am. B* **31**, 259 (2014).
- [121] I. Campillo, J. M. Pitarke, A. Rubio, E. Zarate, and P. M. Echenique, *Phys. Rev. Lett.* **83**, 2230 (1999).
- [122] V. P. Zhukov, E. V. Chulkov, and P. M. Echenique, *Phys. Rev. B* **72**, 155109 (2005).
- [123] G. Baffou and R. Quidant, *Chem. Soc. Rev.* **43**, 3898 (2014).
- [124] H. A. Atwater and A. Polman, *Nat. Mater.* **9**, 865 (2010).
- [125] C. Clavero, *Nat. Photonics* **8**, 95 (2014).
- [126] M. L. Brongersma, N. J. Halas, and P. Nordlander, *Nat. Nanotechnol.* **10**, 25 (2015).
- [127] S. Linic, U. Aslam, C. Boerigter, and M. Morabito, *Nat. Mater.* **14**, 567 (2015).
- [128] R. G. Hobbs, W. P. Putnam, A. Fallahi, Y. Yang, F. X. Kärtner, and K. K. Berggren, *Nano Lett.* **17**, 6069 (2017).
- [129] P. Narang, R. Sundararaman, and H. A. Atwater, *Nanophotonics* **5**, 96 (2016).
- [130] W. Zhu, R. Esteban, A. G. Borisov, J. J. Baumberg, P. Nordlander, H. J. Lezec, J. Aizpurua, and K. B. Crozier, *Nat. Commun.* **7**, 11495 (2016).